



Surface integrity evolution of machined NiTi shape memory alloys after turning process

Yan-Zhe Zhao^{1,2} · Kai Guo^{1,2} · Vinothkumar Sivalingam^{1,2} · Jian-Feng Li^{1,2} · Qi-Dong Sun^{1,2} · Zhao-Ju Zhu^{1,3} · Jie Sun^{1,2}

Received: 12 August 2020 / Revised: 29 September 2020 / Accepted: 11 November 2020 / Published online: 7 January 2021
© Shanghai University and Springer-Verlag GmbH Germany, part of Springer Nature 2021

Abstract Owing to their shape memory effect and pseudoelasticity, NiTi shape memory alloys (SMAs) are widely used as functional materials. Mechanical processes particularly influence the final formation of the product owing to thermal softening and work-hardening effects. Surface integrity is an intermediate bridge between the machining parameter and performance of the product. In this study, experiments were carried out on turning NiTi SMAs at different cutting speeds, where surface integrity characteristics were analyzed. The results show that a higher cutting speed of 125 m/min is required to turn NiTi SMAs based on the evaluation of surface integrity. The degree of work hardening is higher at 15 m/min. Consequently, as a primary effect, work hardening appears on the plastic deformation of the machined samples, leading to dislocations and defects. As the cutting speed increases, the thermal softening effect exceeds work hardening and creates a smoother surface. A stress-induced martensitic transformation is considered during the turning process, but this transformation is reversed to an austenite from the X-ray diffraction (XRD) results. According to the differential scanning calorimetry (DSC) curves, the phase state

and phase transformation are less influenced by machining. Subsequently, the functional properties of NiTi-SMAs are less affected by machining.

Keywords NiTi · Shape memory alloys (SMAs) · Turning · Surface characteristics · Phase transformation · Microhardness

1 Introduction

With the development of modern science and technology on the rise, smart materials have steadily garnered attention owing to their excellent engineering properties. NiTi shape memory alloys (SMAs) are intelligent materials with shape memory and superelasticity, which are widely used in aerospace [1], biomedical [2], automotive, and communication fields [3]. For instance, compared to conventional devices, SMA wires that consist of NiTi SMAs are used to sustain the consistency of actuation modules in wearable prototypes [4], medical-assistant and rehabilitation devices are light weight, silent, and powerful [5]. The SMA thin film actuator provides broader strain recovery, high force to weight ratio, and two-way actuations, which provide prospects for the development of efficient and inexpensive flexible actuators [6]. Owing to their shape memory effects and superelasticity, NiTi thin films are also considered as a promising application in micro-electro-mechanical-systems (MEMS) [7].

However, the unique properties of SMAs also create difficulties in its processing. Both non-conventional and conventional processes have been attempted to obtain better processing quality, such as electro-discharge machining (EDM) [8], laser machining [9], abrasive water-jet machining (AWJ) [10], turning [11], drilling [12], and

✉ Kai Guo
kaiguo@email.sdu.edu.cn

¹ Key Laboratory of High-efficiency and Clean Mechanical Manufacturing, National Demonstration Center for Experimental Mechanical Engineering Education, School of Mechanical Engineering, Shandong University, Jinan 250061, People's Republic of China
² Research Center for Aeronautical Component Manufacturing Technology & Equipment, Shandong University, Jinan 250061, People's Republic of China
³ School of Mechanical Engineering and Automation, Fuzhou University, Fuzhou 350108, People's Republic of China

milling [13]. Furthermore, new machining methods such as additive [14] and laser manufacturing processes [15] have also been applied to the fabrication of NiTi parts. Non-conventional processes appear to have been successfully demonstrated for obtaining NiTi components. However, their rough surfaces, severe heat-affected zones [16], and machining complex geometries limitations, seriously influence the formation of NiTi end products. Additionally, additive manufacturing increases the cost of production. Consequently, conventional machining remains a suitable method for fabricating NiTi SMA components [17]. Moreover, NiTi SMAs are classified as difficult-to-machine materials because of their high ductility, tool wear, and work-hardening behavior [18].

The machining process plays a vital role in forming the final product. Simultaneously, surface integrity directly influences the quality and performance of the product. It is well known that high temperatures and a high strain rate exist in the cutting process, thus affecting the machined materials. The phase transformation behavior occurs when the NiTi SMAs undergo heating and cooling, whereas the stress-induced martensitic phase appears when loading NiTi SMAs above the austenite finish temperature (A_f). Consequently, because they are temperature-sensitive and phase-changeable materials, the effects of thermo-mechanical coupling on the machined NiTi SMAs should be considered after machining.

Recently, many researchers have analyzed the surface integrity of the components of machined NiTi SMAs. Wu et al. [19] performed a cutting Ti49.6Ni50.4-alloy experiment using a precision saw, and stated that the strain and fatigue hardenings during cutting were the reasons for the broad hardening layer forms in the Ti49.6Ni50.4 alloy. Pits and ploughing grooves have emerged on the surface morphologies owing to the adhesion of the material to the diamond blade. Weinert and Petzoldt [20] performed a drilling experiment on a martensitic alloy. It was concluded that the work-hardening layer decreased as the cutting speed increased, and the increased feed rate promoted the formation of the work-hardening layer. This occurred due to the detwinned martensite that appeared after drilling, which increased the hardness. Guo et al. [21] compared the surface integrity of milling to the EDM of nitinol alloy and concluded that the roughness on the machined surface after milling was lower than that after the EDM trim cut. The white layer generated on the subsurface in milling is the austenite created by large deformation while the thick white layers are produced by melting and rapid quenching in the EDM process. Kaynak et al. [11] carried out a series of experiments on turning NiTi alloys and concluded that machining altered the room-temperature phase in machined NiTi alloy samples. The latent heat of transformation also decreased after machining. Cryogenic machining

dramatically influenced the phase state and phase transformation temperature while the A_f temperature increased by 27% and 29% at low and high cutting speeds, respectively. Wang et al. [22] carried out a milling experiment on Ni50.8Ti49.2 SMAs, and analyzed the hardening degree, hardening depth, and diffraction peak after the milling process. The results demonstrated that the cutting speed and feed significantly impacted strain hardening. The depth of the induced layer increased as the hardening degree increased while the diffraction peak increased with increasing cutting speed. Zainal et al. [23] performed micro-milling tests on NiTi SMAs, and stated that a machined subsurface under cold air plus a minimum quantity lubricant (MQL) condition could greatly reduce burrs. The finest surface roughness can be obtained when the tool radius is smaller than the uncut chip thickness. Meanwhile, the surface integrity of the machined surface is also an interesting characteristic to consider after non-conventional processes are performed. Kong et al. [10] employed the multi-mode abrasive waterjet machining of NiTi and concluded that the white layer, deformed structure, and cracks were not present on the machined workpiece. The generated surface can satisfy quality requirements, as the roughness of the cut surface and that on the miller surface are less than 4 μm and 5 μm , respectively. Liu et al. [24] explored surface integrity according to wire electrode discharge machining (W-EDM) by trim and main cuts. Roughness is influenced by the thickness of the sample and machined method. There are micro-voids, micro-cracks, and a discontinuous porous white layer in the main cut while elemental diffusion occurred during machining. Huang et al. [25] applied EDM to a TiNi-based SMA and concluded that recast materials and electrical discharge craters existed on the EDMed surface. Even with the high surface hardness in the recast layers, the SMAs still exhibit functional recovery.

According to these studies, the surface roughness, microstructure, hardness, and phase transition of the surface integrity characteristic were investigated. Studies have explored a suitable NiTi SMA product that satisfies quality requirements. For a comprehensive and systematic analysis of machined surface integrity, an experiment on turning NiTi SMAs at different cutting speeds was carried out in this study. Regarding the phase transformation properties of NiTi SMAs, the surface roughness, microstructures, microhardness, and phase relative characteristics were analyzed in this study. Meanwhile, to better understand the relationship between cutting speed and the product performance induced by machining, the influence of cutting speed on surface integrity was investigated.

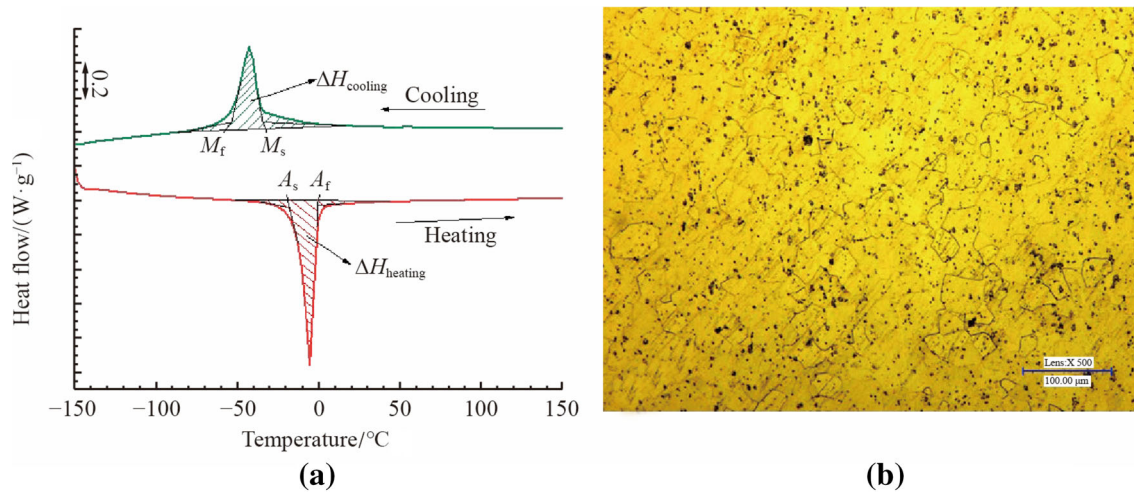


Fig. 1 **a** DSC curve of NiTi SMAs, **b** microstructure of the as-received specimen

2 Experimental procedure

2.1 Workpiece material

The material used in this experiment was a Ni50.8Ti (atom fraction) SMA bar with a 20 mm diameter under hot forging conditions, which was provided by Baoji Runyang Rare Metals Limited, China. The EDM machine produced by Taizhou poussy CNC machine technology LTD was used to cut the long bar to small pieces of 60 mm lengths. The NiTi SMAs were in the austenitic phase at room temperature, as measured by the Netzsch DSC3500 Sirius equipment at a heating/cooling rate of 10 °C/min. The phase transition temperature and latent heat of phase transformation during cooling ($\Delta H_{\text{cooling}}$) and heating ($\Delta H_{\text{heating}}$) are shown in the differential scanning calorimetry (DSC) curve in Fig. 1a. From the DSC curve, the martensite finish (M_f), martensite start (M_s), austenite start (A_s), and austenite finish (A_f) temperatures are -53 °C, -35 °C, -13 °C and -2 °C, respectively. Additionally, $\Delta H_{\text{heating}}$ and $\Delta H_{\text{cooling}}$ are 20.15 J/g and 17.5 J/g, respectively. A digital optical microscope (KEYENCE VHX-600) was used to examine the microstructure of the as-received specimen, as shown in Fig. 1b.

The physical and mechanical properties of NiTi SMAs are presented in Table 1 [26].

2.2 Turning process

The experiment was performed on a C6140H turning machine under dry conditions. Because inserts with TiAlN coating are more suitable for machining NiTi SMAs [27], the cutting insert used in this experiment was a PVD-coated carbide insert (VNMG160408-SM1105) with TiAlN coatings. Five cutting speeds (v_c) were selected: 15, 33, 47,

Table 1 Physical and mechanical properties of NiTi SMAs

Property	NiTi SMAs	
	Austenite	Martensite
Density/($\text{kg}\cdot\text{m}^{-3}$)	6 450	
Conductivity/($\text{W}\cdot(\text{m}\cdot^\circ\text{C})^{-1}$)	18 (20 °C)	8.5 (20 °C)
Expansion/ $\times 10^{-6}$	11.3 (20 °C)	6.6 (20 °C)
Melting temperature/°C	1 240	
Young's modulus/GPa	83 (20 °C)	41 (20 °C)
Poisson's ratio	0.3	
Specific heat/($\text{J}\cdot(\text{kg}\cdot^\circ\text{C})^{-1}$)	837.36 (20 °C)	
Yield strength/MPa	195–690	70–140
Tensile strength/MPa	80–1 500	700–1 100

Table 2 Experimental details

Items	Descriptions
Workpiece	NiTi SMA
Cutting tool	VNMG160408-SM1105, Sandvick
Cutting speed (v_c)/($\text{m}\cdot\text{min}^{-1}$)	15, 33, 47, 87, 125
Feed rate (f)/($\text{mm}\cdot\text{r}^{-1}$)	0.15
Depth of cut (a_p)/mm	0.2

87 and 125 m/min. The feed rate (f) and depth of cut (a_p) were kept constant at 0.15 mm/r and 0.2 mm, respectively. The experimental details are shown in Table 2.

Each cutting test sample had a length of 10 mm, and a new insert was used in every test to eliminate the effect of tool wear. The schematic diagram of turning is shown in Fig. 2.

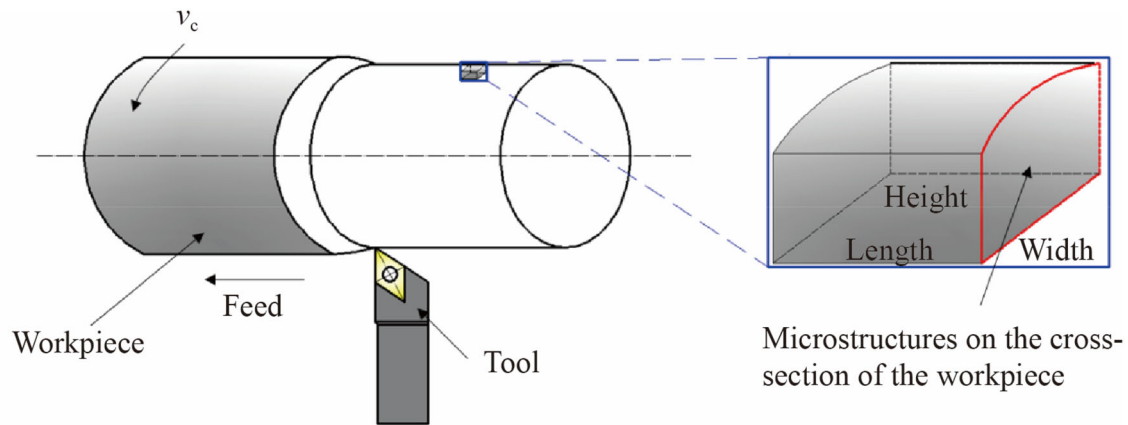


Fig. 2 Schematic of turning and the cross-section of the workpiece

2.3 Measurement of NiTi SMA characteristics before and after turning

The machined surface morphology was examined using a digital optical microscope (KEYENCE VHX-600) and an optical profiler (Veeco NT9300, USA). The average surface roughness (R_a) was obtained from the same optical profiler and computed using the WYKO Vision 32 software. Ultima IV observed the phase state on the surface of the as-received and machined samples. The scan speed was 10 °C/min within the range of 20°–80° 2θ scans at room temperature to obtain the X-ray diffraction (XRD) patterns. The XRD peak positions and corresponding 2θ degrees were determined by lattice parameters, $a_0 = 0.2998$ nm, for the austenite phase from the powder diffraction file (PDF) in a Jade software.

The as-received and machined samples at different cutting speeds were cut into 5 mm × 5 mm × 5 mm by EDM, as shown in Fig. 2. After the cold mounting and polishing process, the machined and as-received samples were polished to measure the microhardness. The MH-6 Vickers digital microhardness tester measured the microhardness with a load of 50 g and a dwelling time of 10 s.

The phase transformation characteristics of the machined samples were obtained by the Netzsch DSC3500 Sirius at a heating/cooling rate of 10 °C/min. Because the EDM process caused the heat-affected area on the machined pieces [28], the DSC samples cut by EDM were polished using an abrasive paper [11]. The thickness of the DSC sample was 1 mm, and its quality was controlled between 10 mg and 50 mg.

3 Results and discussion

3.1 Surface characteristics

3.1.1 Surface roughness

Surface roughness is a primary indicator of the quality of the surface finish [29]. It is widely characterized by the average surface roughness (R_a), which affects the functionality of manufactured products [30]. Figure 3 presents the R_a values at different cutting speeds. The R_a obtained in this experiment is less than 1.6 μm , which meets the quality requirements of NiTi manufacturing parts for the aerospace industry [10]. Furthermore, the smallest surface roughness obtained was 0.3 μm at a cutting speed of 125 m/min.

The R_a increased with an increase in the cutting speed at cutting speeds less than 47 m/min but slightly decreased as the cutting speed increased (more than 47 m/min). Similar to the low thermal conductivity and high ductility of NiTi SMAs presented in Table 1, some materials adhere to the cutting edge at high cutting temperature, forming the built-up edge (BUE) within the cutting speed of 47 m/min. In this period, because of work hardening, the formed BUE becomes hard and leads to more instability [31]. The formation and disappearance of BUE, together with frictional rubbing, make the surface finish worse [32]. The surface of the ups and downs in one feed in the three-dimensional (3D) surface topography at a cutting speed of 15 m/min, as shown in Fig. 3, also confirms that with an increase in the cutting speed up to less than 47 m/min, the increased tool wear and BUE, as well as the increased cutting temperature, the surface finish became worse.

With the cutting speed increasing to 87 m/min, the cutting temperature was higher, causing the thermal softening effect to exceed the hardening effect. Together with

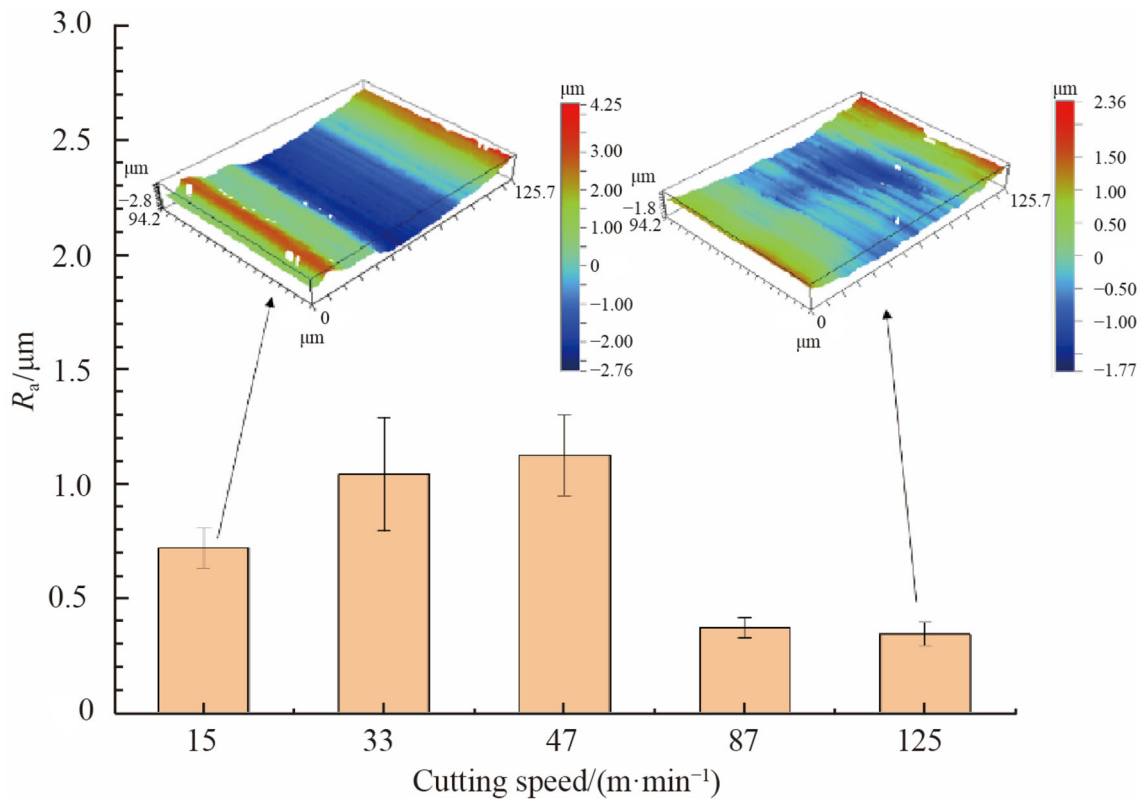


Fig. 3 Average surface roughness at different cutting speeds and 3D surface topography at typical cutting speeds

the decrease in friction coefficients at higher cutting temperatures, the surface roughness decreases at a lower cutting speed. Consequently, the surface is significantly smoother in one feed from the 3D surface topography at a cutting speed of 125 m/min, as shown in Fig. 3. Surface roughness decreases slightly as cutting speed increases, which is caused by the smoothing of the nose profile by adhesion wear [17, 33].

3.1.2 Surface morphology

Surface morphology is a characteristic of surface integrity. Figure 4 shows the optical morphology images of the machined surface after turning at different cutting speeds. There were feed marks, metal debris, long grooves, and smeared material on the machined surface. Feed marks can be observed on the machined surface at lower cutting speeds (less than 47 m/min). In contrast, the BUE formation and disappearance result in regular grooves with different heights. However, plastic deformation is dominated by the mechanical effect at lower cutting speeds (less than 47 m/min). As the cutting temperature increases with the cutting speed, an increasing amount of plastic deformation occurs on the machined surface, which leads to the gradual deformation of the feed marks [32]. Furthermore, with the process of turning, the BUE detaches from the tool and is

transferred to the machined surface, which leads to metal debris [34].

With an increase in cutting speed, thermal softening increased; BUE was removed; and cutting force was reduced, which weakened the negative effect of plastic deformation on the machined surface. Better surface quality and fewer defects were observed at higher cutting speeds (more than 87 m/min). When the cutting speed was increased to 87 m/min, the long grooves and smeared materials appeared on the machined surface, and the tool wear created long grooves at a higher cutting speed. Because plastic deformation is dominated by the thermal effect, localized high temperature at the tool-workpiece contact area leads to smeared materials on the machined surface [35]. The plastic flow of the work material at a high temperature easily embeds or sticks to metal debris [32, 36].

From the results of the surface characteristics at different cutting speeds, there is a significant difference in the surface integrity between lower cutting speeds (less than 47 m/min) and higher cutting speeds (more than 87 m/min) at the cutting speed range in this experiment. Ultimately, for the machining process, the mechanical effect of high stress and strain, including the thermal effect caused by high temperature and quenching, are the main reasons for the alterations in surface integrity [34]. A low cutting speed

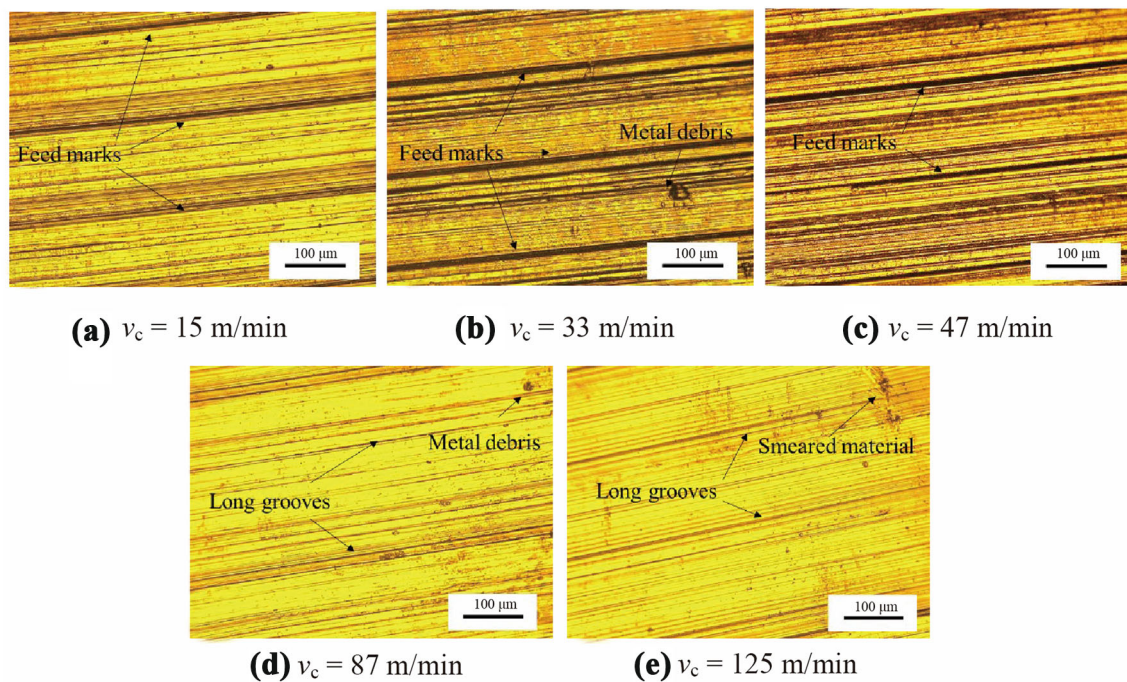


Fig. 4 Surface morphology images of machined surface at different cutting speeds

of 15 m/min is mainly subject to a mechanical effect, and the thermal effect is the primary effect on the machined surface at a high cutting speed of 125 m/min. Therefore, the following analysis will focus on other surface integrity features at two typical cutting speeds: 15 m/min and 125 m/min.

3.2 Microstructure

The thermal and mechanical effects on the machined workpiece during the cutting process lead to microstructural changes in the material. The microstructures of the cross-section of the machined sample at two typical cutting speeds are shown in Fig. 5. The deforming lines cannot be observed in Fig. 5a, although they are evenly distributed on the subsurface, as shown in Fig. 5b. The cutting speed of 15 m/min is a lower cutting speed with lower cutting temperature, and plastic deformation is mainly caused by mechanical effects. Together with the uneven surface created by BUE, the deformation at the part of the cross-sections near the surface is irregular. Consequently, the grain boundaries of the deformation region are not as visible as most of the workpiece [37]. The deformation of the sub-surface material can be seen at 125 m/min, and the deformation direction is consistent with the cutting speed. The deformation zone is about 10 μm in depth from the surface, indicating severe plastic deformation in this area. As the cutting temperature increases with the cutting speed, the thermal effect also increases correspondingly. Plastic

deformation is mainly generated by the thermal effect on the machining area at 125 m/min. Stress flow can be clearly observed in the deformed zone. Meanwhile, the grain boundaries were fined at a cutting speed of 125 m/min, as the residual stress was released.

3.3 Phase state and phase transformation temperature

3.3.1 Phase state from XRD

Because NiTi SMAs are sensitive to temperature and stress, mechanical and thermal effects significantly influence the properties of the material during machining. XRD pattern is a direct and straightforward approach to obtaining the phase state of the workpiece. Figure 6 shows the XRD patterns of the as-received and machined surfaces at speeds of 15 m/min and 125 m/min, respectively. Only austenite (B2) diffraction peaks exists with (110), (200), and (211) Miller indices in the picture. Because the A_f temperature of the received-one is $-2\text{ }^\circ\text{C}$, the phase state is independent of the higher cutting temperature. However, a stress-induced martensite phase occurs during machining, which is caused by loading. The stress-induced martensite phase appeared during machining, and the reverse transformation of martensite to austenite occurred thoroughly after unloading. The turning process does not influence the phase state on the surface.

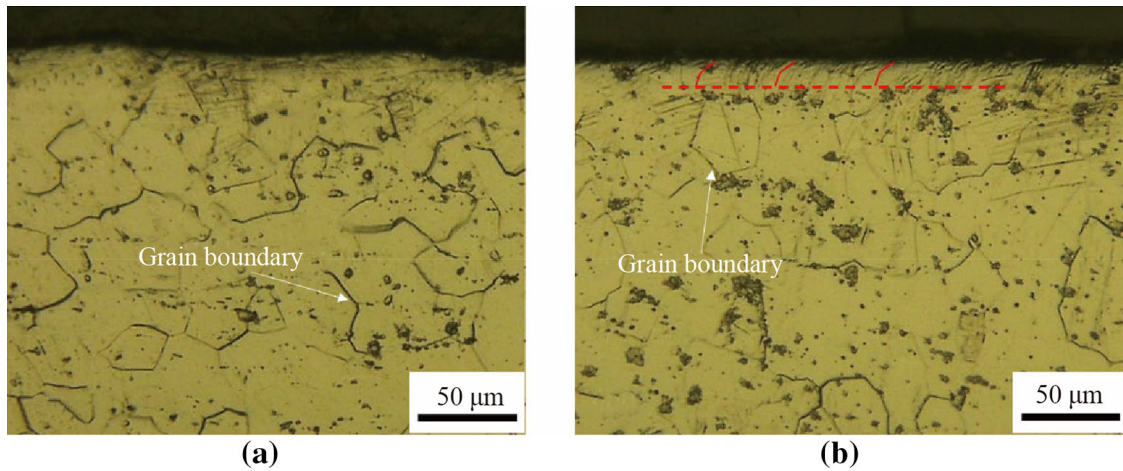


Fig. 5 Microstructures of cross-sections of the machined surface at the cutting speed of **a** 15 m/min, **b** 125 m/min under f of 0.15 mm/r and a_p of 0.2 mm

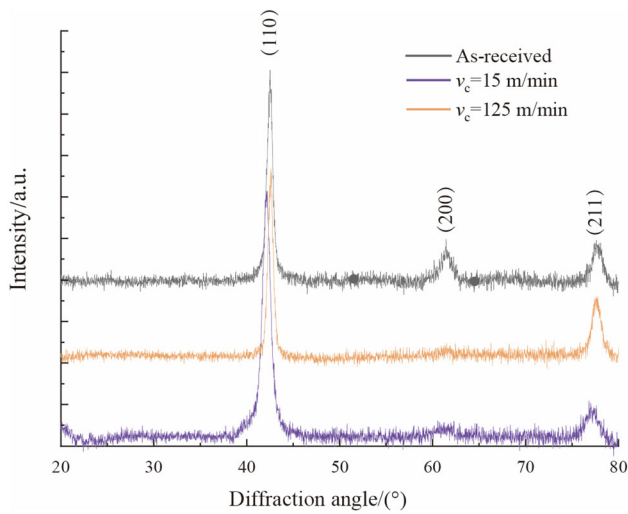


Fig. 6 XRD patterns of the as-received and machined surface at the speeds of 15 m/min and 125 m/min

However, the diffraction peak with the (200) Miller index is severely weakened after machining. Compared to the as-received one, the diffraction peak with the (110) Miller index is broader and higher at a cutting speed of 15 m/min, whereas it is lower at a cutting speed of 125 m/min. This result indicates that the microstructure is altered on the machined surface. Kaynak [38] explained that during the cutting process at low cutting speed, the mechanical effect was the primary effect, which increased the dislocation density and defects in the microstructure. Therefore, the peak broadening is distinctly observed. The dislocation density and stress are reduced by the high cutting temperature at higher cutting speeds, leading to considerable peak broadening.

The full width at half maximum (FWHM) is the critical factor for calculating the grain size and characterizing the

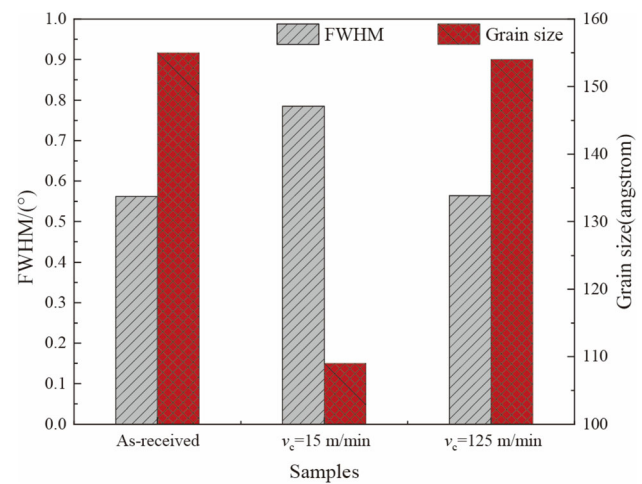


Fig. 7 FWHM and grain size at different cutting speeds

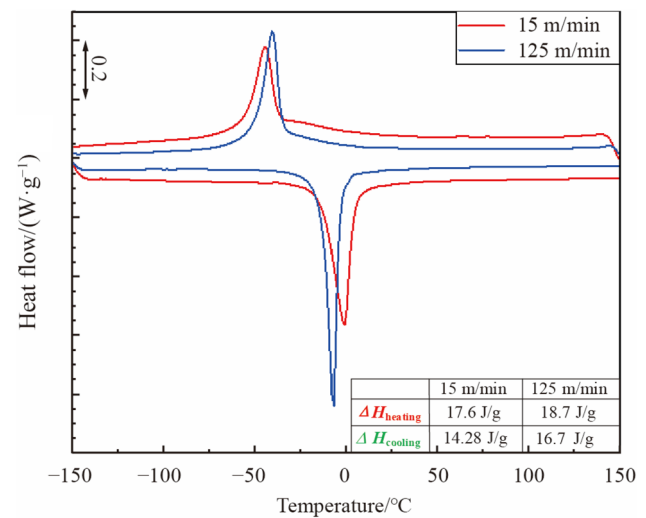


Fig. 8 DSC curves of machined samples at two cutting speeds

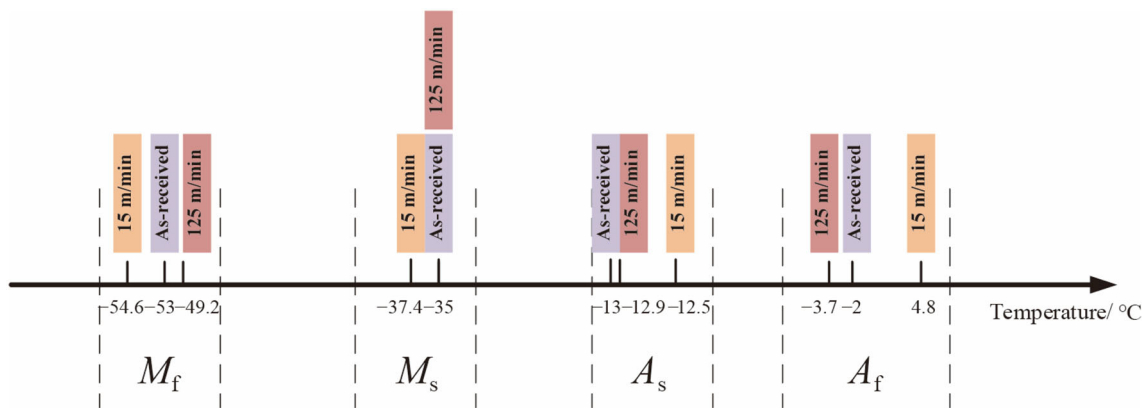


Fig. 9 Phase transition temperature of as-received and machined samples

hardening of the material during processing. The FWHM and estimated grain size from the diffraction peak with the (110) Miller index was calculated using Jade software based on the Scherrer formula [39], as shown in Fig. 7. At 125 m/min, the influence of the FWHM and grain size on the machined surface is negligible. The FWHM of the machined surface at 15 m/min was more significant than that at 125 m/min. This result indicates that the hardness on the surface is harder at low cutting speeds than at high cutting speeds. This is because the effect of work hardening is more significant than the thermal effect at low cutting speeds. The cutting temperature increases with an increase in cutting speed, which causes the thermal effect to exceed work hardening. The grain size was smaller at 15 m/min than at 125 m/min. This result corresponds to the peak in Fig. 6, thus indicating a uniform and grain-refined microstructure on the surface at low cutting speeds.

3.3.2 Phase transformation from the DSC curve

Phase transformation is a unique property of SMAs. It is directly related to the martensitic phase transition, which affects the shape memory effect and pseudoelasticity. The DSC curve provides information related to the phase transformation. Figure 8 shows the phase transformation of machined samples at cutting speeds of 15 m/min and 125 m/min.

From the information observed in Figs. 8 and 9, it is clear that machining affects the DSC response [40]. The latent heat of phase transformation after machining is smaller than that of the as-received one. This is because the dislocation in machined samples inhibits phase transformation in some of the materials [41], leading to less energy for phase transformation [11]. Because the drop in latent heat at 15 m/min is more significant than that at 125 m/min, there is a higher dislocation density in machined samples at low cutting speed. These results agree with the

XRD patterns, thus indicating that more dislocations occurred at lower cutting speed.

Meanwhile, from the phase transition temperature shown in Fig. 9, the change in the phase transition temperature before and after machining is insignificant, less than 10 °C. At a speed of 125 m/min, the phase transition temperature remains almost unchanged. The hysteresis of the phase transformation occurs at a speed of 15 m/min, thus suggesting that the phase transformation resistance increases and influences the shape memory effect to some extent. This is because the mechanical effect leads to residual stress and high dislocation in the machined samples [37].

3.4 Microhardness

Severe work hardening is a principal aspect of turning NiTi SMAs, and it has an adverse effect on the shape memory effect and pseudoelasticity [13]. As an indicator of the

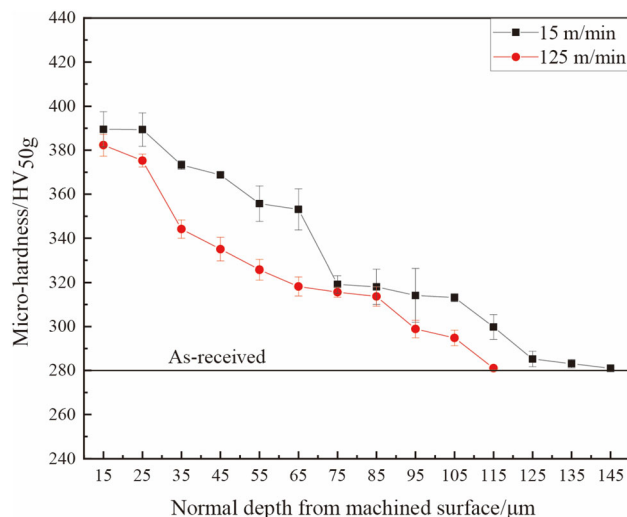


Fig. 10 Microhardness on the subsurface

degree of work hardening, microhardness is an integral part of surface integrity. The microhardness on the subsurface is shown in Fig. 10. The microhardness of the as-received sample was 280 HV. The maximum micro-hardness value was 385 HV at a cutting speed of 15 m/min. It is clear that the degree of work hardening is lower at high cutting speeds than that at low cutting speeds, and the depths of the work-hardening layers are 115 μm and 145 μm at 15 m/min and 145 m/min, respectively. Plastic deformation leading to work hardening, together with the mechanical and thermal effects are essential factors that affect plastic deformation [42]. The mechanical hardening effect was greater than the thermal softening effect at 15 m/min. In comparison, the thermal softening effect exceeds the work hardening at 125 m/min because a high cutting speed triggers a high temperature. Consequently, the degree of work hardening was higher at 15 m/min than at 125 m/min.

4 Conclusions

Surface and sub-surface characteristics are closely related to the fatigue, friction, and corrosion properties of the workpiece. The relative parameters of the phase influence the shape memory effect and pseudoelasticity of NiTi SMAs. These parameters are all affected by machining. Therefore, the surface integrity of machined samples after dry turning them on NiTi SMAs was analyzed in this work, and the conclusions drawn from these investigations are as follows.

- (i) Mechanical effect is the dominant factor that influences surface integrity at low cutting speeds while thermal effect is the dominant factor at high cutting speeds.
- (ii) Turning at a speed of 125 m/min achieves a lower surface roughness of 0.3 μm . The influence of that turning speed on the phase state and phase transformation is negligible, which means that it has an insignificant effect on the functional properties of NiTi SMAs.
- (iii) There were more dislocations and defects in the machined samples after turning at a speed of 15 m/min, leading to low surface characteristics and changes in phase characteristics.
- (iv) Work hardening is more significant at low cutting speeds than at high cutting speeds. Considering surface integrity, a high cutting speed of 125 m/min is the appropriate cutting speed in this study.

Acknowledgements This work was supported by the National Natural Science Foundation of China (Grant No. 51975335), the

Construction Engineering Special Fund of “Taishan Scholars” of the Shandong Province (Grant No. 20190975), the Fundamental Research Funds of Shandong University (Grant No. 2019HW040), and the Key Laboratory of High-efficiency and Clean Mechanical Manufacture at Shandong University, Ministry of Education.

References

1. Bil C, Massey K, Abdullah EJ (2013) Wing morphing control with shape memory alloy actuators. *J Intell Mater Syst Struct* 24:879–898
2. Petrini L, Migliavacca F (2011) Biomedical applications of shape memory alloys. *J Metall*. <https://doi.org/10.1155/2011/501483>
3. Kaya E, Kaya İ (2020) Tool wear progression of PCD and PCBN cutting tools in high speed machining of NiTi shape memory alloy under various cutting speeds. *Diam Relat Mater*. <https://doi.org/10.1016/j.diamond.2020.107810>
4. Hope J, McDaid A (2017) Development of wearable wrist and forearm exoskeleton with shape memory alloy actuators. *J Intell Robot Syst Theory Appl* 86:397–417
5. Nematollahi M, Baghbaderani KS, Amerinatanzi A et al (2019) Application of NiTi in assistive and rehabilitation devices: a review. *Bioeng*. <https://doi.org/10.3390/bioengineering6020037>
6. Jayachandran S, Akash K, Mani Prabu SS et al (2019) Investigations on performance viability of NiTi, NiTiCu, CuAlNi and CuAlNiMn shape memory alloy/Kapton composite thin film for actuator application. *Compos Part B Eng* 176:107182. <https://doi.org/10.1016/j.compositesb.2019.107182>
7. Mehrpouya M, Bidsorkhi HC (2017) MEMS applications of NiTi based shape memory alloys: a review. *Micro Nanosyst* 8:79–91
8. Hsieh SF, Hsue AWJ, Chen SL et al (2013) EDM surface characteristics and shape recovery ability of Ti35.5Ni48.5Zr16 and Ni60Al 24.5Fe15.5 ternary shape memory alloys. *J Alloys Compd* 571:63–68
9. Pfeifer R, Herzog D, Hustedt M et al (2010) Pulsed Nd:YAG laser cutting of NiTi shape memory alloys—influence of process parameters. *J Mater Process Technol* 210:1918–1925
10. Kong MC, Srinivasu D, Axinte D et al (2013) On geometrical accuracy and integrity of surfaces in multi-mode abrasive waterjet machining of NiTi shape memory alloys. *CIRP Ann Manuf Technol* 62:555–558
11. Kaynak Y, Huang B, Karaca HE et al (2017) Surface characteristics of machined NiTi shape memory alloy: the effects of cryogenic cooling and preheating conditions. *J Mater Eng Perform* 26:3597–3606
12. Weinert K, Petzoldt V, Kötter D (2004) Turning and drilling of NiTi shape memory alloys. *CIRP Ann Manuf Technol* 53:65–68
13. Wang G, Liu Z, Niu J et al (2019) Work hardening influencing on shape memory effect of NiTi alloy by varying milling speeds. *Smart Mater Struct*. <https://doi.org/10.1088/1361-665X/ab3de2>
14. Elahinia M, Shayesteh MN, Taheri AM et al (2016) Fabrication of NiTi through additive manufacturing: a review. *Prog Mater Sci* 83:630–663
15. Mehrpouya M, Gisario A, Elahinia M (2018) Laser welding of NiTi shape memory alloy: a review. *J Manuf Process* 31:162–186
16. Huang H, Zheng HY, Liu Y (2005) Experimental investigations of the machinability of Ni50.6Ti49.4 alloy. *Smart Mater Struct*. <https://doi.org/10.1088/0964-1726/14/5/019>
17. Kaynak Y, Karaca HE, Noebe RD et al (2013) Tool-wear analysis in cryogenic machining of NiTi shape memory alloys: a comparison of tool-wear performance with dry and MQL machining. *Wear* 306:51–63

18. Hassan MR, Mehrpouya M, Dawood S (2014) Review of the machining difficulties of nickel-titanium based shape memory alloys. *Appl Mech Mater* 564:533–537
19. Wu SK, Lin HC, Chen CC (1999) Study on the machinability of a Ti49.6Ni50.4 shape memory alloy. *Mater Lett* 40:27–32
20. Weinert K, Petzoldt V (2004) Machining of NiTi based shape memory alloys. *Mater Sci Eng A* 378:180–184
21. Guo Y, Klink A, Fu C et al (2013) Machinability and surface integrity of nitinol shape memory alloy. *CIRP Ann Manuf Technol* 62:83–86
22. Wang G, Liu Z, Ai X et al (2018) Effect of cutting parameters on strain hardening of nickel-titanium shape memory alloy. *Smart Mater Struct*. <https://doi.org/10.1088/1361-665X/aac43d>
23. Zainal AZ, Tarisai MP, Harrison G (2020) Chilled air system and size effect in micro-milling of nickel-titanium shape memory alloys. *Int J Precis Eng Manuf Green Technol* 7:283–297
24. Liu JF, Li L, Guo YB (2014) Surface integrity evolution from main cut to finish trim cut in W-EDM of shape memory alloy. *Procedia CIRP* 13:137–142
25. Huang TS, Hsieh SF, Chen SL et al (2015) Surface modification of TiNi-based shape memory alloys by dry electrical discharge machining. *J Mater Process Technol* 221:279–284
26. Zhao Y, Li J, Guo K et al (2020) Study on chip formation characteristics in turning NiTi shape memory alloys. *J Manuf Process* 58:787–795
27. Mehrpouya M, Shahedin AM, Daood SDS et al (2017) An investigation on the optimum machinability of NiTi based shape memory alloy. *Mater Manuf Process* 32:1497–1504
28. Dash B, Das M, Das M et al (2019) A concise review on machinability of NiTi shape memory alloys. *Mater Today Proc* 18:5141–5150
29. Ulutan D, Ozel T (2011) Machining induced surface integrity in titanium and nickel alloys: a review. *Int J Mach Tools Manuf* 51:250–280
30. Deltombe R, Kubiak KJ, Bigerelle M (2014) How to select the most relevant 3D roughness parameters of a surface. *Scanning* 36:150–160
31. Sivalingam V, Sun J, Yang B et al (2018) Machining performance and tool wear analysis on cryogenic treated insert during end milling of Ti-6Al-4V alloy. *J Manuf Process* 36:188–196
32. Thakur A, Mohanty A, Gangopadhyay S (2014) Comparative study of surface integrity aspects of Incoloy 825 during machining with uncoated and CVD multilayer coated inserts. *Appl Surf Sci* 320:829–837
33. Dhar NR, Kamruzzaman M (2007) Cutting temperature, tool wear, surface roughness and dimensional deviation in turning AISI-4037 steel under cryogenic condition. *Int J Mach Tools Manuf* 47:754–759
34. Thakur A, Gangopadhyay S (2016) State-of-the-art in surface integrity in machining of nickel-based super alloys. *Int J Mach Tools Manuf* 100:25–54
35. Arunachalam RM, Mannan MA, Spowage AC (2004) Surface integrity when machining age hardened Inconel 718 with coated carbide cutting tools. *Int J Mach Tools Manuf* 44:1481–1491
36. Zou B, Chen M, Huang C et al (2009) Study on surface damages caused by turning NiCr20TiAl nickel-based alloy. *J Mater Process Technol* 209:5802–5809
37. Kaynak Y, Karaca HE, Jawahir IS (2014) Surface integrity characteristics of NiTi shape memory alloys resulting from dry and cryogenic machining. *Procedia CIRP* 13:393–398
38. Kaynak Y (2014) Machining and phase transformation response of room-temperature austenitic NiTi shape memory alloy. *J Mater Eng Perform* 23:3354–3360
39. Wang G, Liu Z, Niu J et al (2020) Effect of electrochemical polishing on surface quality of nickel-titanium shape memory alloy after milling. *J Mater Res Technol* 9:253–262
40. Kaynak Y, Tobe H, Noebe RD et al (2014) The effects of machining on the microstructure and transformation behavior of NiTi alloy. *Scr Mater* 74:60–63
41. Miller DA, Lagoudas DC (2000) Thermomechanical characterization of NiTiCu and NiTi SMA actuators: influence of plastic strains. *Smart Mater Struct* 9:640–652
42. Arunachalam RM, Mannan MA, Spowage AC (2004) Residual stress and surface roughness when facing age hardened Inconel 718 with CBN and ceramic cutting tools. *Int J Mach Tools Manuf* 44:879–887



Yan-Zhe Zhao is a Ph.D. candidate of Mechanical Engineering at Shandong University, Jinan, China. Her current research includes properties of NiTi shape memory alloys, advanced manufacturing technology, and green manufacturing.



Kai Guo received his Ph.D. degree in fluid power transmission and control from Zhejiang University, Hangzhou, China, in 2015. He is currently an assistant professor of Mechanical Engineering, Shandong University, China. His current research interests include advanced manufacturing, machining, and the modeling hydraulic component.

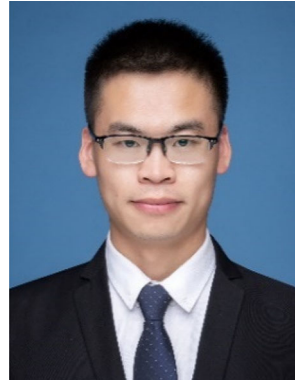


Vinothkumar Sivalingam has a Ph.D. in Mechanical Engineering and works as an associate professor at the School of Mechanical Engineering, Shandong University, China. He has approximately 6 years of teaching and research experience. He has published 10 research papers in international journals, and his research field encompasses advanced machining processes and green manufacturing.



Jian-Feng Li received his Ph.D. degree in Mechanical Engineering from Shandong University, Jinan, China, in 1994. He is currently a professor of Mechanical Engineering at Shandong University, Jinan, China. He has implemented several projects from the National Nature Science Foundation, and two projects from the 973 Program. He has authored or coauthored more than 100 journal and conference papers. His current research

interests include advanced and green manufacturing.



Zhao-Ju Zhu received his Ph.D. degree in mechanical engineering from Shandong University, China, in 2019. He currently holds a lecture position at Fuzhou University and a postdoctoral position at the Institute of Automation, Chinese Academy of Sciences. His research interests include advanced manufacturing and data analysis.



Qi-Dong Sun is a M.Sc. candidate of Mechanical Engineering at Shandong University, Jinan, China. His current research includes properties of the Ti-6Al-4V alloy and additive manufacturing.



Jie Sun received his Ph.D. degree in Mechanical Engineering from Zhejiang University, Hangzhou, China, in 2004. He is a professor and head of the Research Centre for Aeronautical Component Manufacturing Technology and Equipment in Shandong University, China. His current research interests include advanced manufacturing, aerospace manufacturing, and additive manufacturing.